Development, Uniformity and Peak Heating of a Hypersonic Laminar Near-Wake Flow

S. O'Byrne[1] and P. M. Danehy[2]
[1]University of New South Wales, Canberra, A.C.T., 2600 Australia.
[2]NASA Langley Research Center, Hampton, VA, 23681, USA

Abstract

This paper describes visualisation experiments performed using the planar laser-induced fluorescence of nitric oxide. The focus was to investigate the establishment and cross-stream uniformity of the hypersonic separated flow generated in a pulsed free-piston shock tunnel facility. In particular, the laminar Mach 7.5 flow over a step downstream of a wedge was investigated. The ratio of wedge width to total horizontal distance downstream of the leading edge was 0.71 at the furthest downstream measurement point, and model side plates were not used. Flow images were obtained on successive tunnel runs with different delays after flow onset, to identify the nominal flow establishment time. Furthermore, images were obtained at the nominal facility test time using a laser sheet oriented perpendicular to the step, propagating in the spanwise direction at a height equal to half the step height. These images are compared with thermocouple heat flux measurements obtained both with and without the step and show that while the flow downstream of reattachment is uniform in the middle of the model, the separated flow immediately downstream of the step is non-uniform.

NOMENCLATURE

c	specific heat
h	step height
H	enthalpy
k	thermal conductivity
L	length along the upper wedge surface between leading edge and expansion corner
M	Mach number
p	pressure
$\dot{q}$	heat flux
Re_L	Reynolds number based on length L
T	temperature
u	velocity
ρ	density

Subscripts

∞	freestream
0	at stagnation conditions
fp	property measured for the same position downstream of the wedge using zero step height.

1. INTRODUCTION

Two-dimensionality is a useful simplifying assumption for formulating mathematical descriptions of flow behaviour. Experiments are routinely designed to allow this idealisation to be made. It is, however, difficult to generate a truly two-dimensional flowfield, particularly if it contains large regions of subsonic separated flow. Unless experiments are designed with care, it may be unclear whether disagreements between experimental results and theory are caused by an inadequacy of theory or by failure of the experiment to generate a flow which conforms to the theory's assumptions.

It may not be easy or practical to place surface transducers with sufficient density to accurately determine the two-dimensionality of flow at the surface of a model. Even in cases where the placement

of surface transducers is sufficiently dense, flow two-dimensionality is only measured at the model surface. This paper describes an experiment using a spatially-resolved imaging technique, planar laser-induced fluorescence (PLIF), to visualise the separated re- gion downstream of a wedge in a hypersonic freestream. The imaging is non-intrusive and provides high-resolution sampling of the flow, indicating regions of non-uniform temperature and density. The images provide information about two-dimensional regions within the flow field and are not restricted to measuring surface distributions. In this experiment, fluorescence images of the flow are obtained and compared with surface heat-flux measurements. Both measurements are used to provide an indication of flow two-dimensionality.

As well as providing a comparison with the fluorescence images, peak heat flux is measured in the separated region and compared with the heat flux for an equivalent attached boundary layer. The results of this comparison are also compared with heat flux measurements obtained at similar conditions by other investigators.

2. EXPERIMENT

2.1. Facility, Flow Conditions and Model

The experiments were performed using the T2 free-piston shock tunnel facility [1] at the Australian National University. Free-piston shock tunnels generate very high shock speeds by the near-adiabatic free-piston compression of a monatomic driver gas. This compression process generates a shock wave by bursting a steel diaphragm separating the driver and test gases. The high-pressure and high-temperature nozzle plenum conditions are generated by the reflection of this shock wave from the end wall of a shock tube that terminates in a conical converging-diverging nozzle. The test gas used in these experiments was a mixture of 1% oxygen in nitrogen. This mixture reacts in the nozzle reservoir, generating a mole fraction of approximately 1% nitric oxide (NO), which is used as the seed gas for the planar laser- induced fluorescence (PLIF) visualisations. The proportion of molecular oxygen in the mixture was small enough to not cause significant absorption of the laser sheet at these flow conditions. The conical nozzle had a physical half-angle of 7.5 $^\circ$ and an exit-to-throat area ratio of 183, producing the nozzle exit conditions shown in Table 1. Freestream flow conditions were calculated from measured nozzle reservoir pressure, shock speed and pitot pressure, using an equilib- rium shock tube code [2] and a 1-dimensional chemical nonequilibrium nozzle calculation [3]. The pitot pressure indicated that the boundary layer in the nozzle reduces the expansion in the nozzle to an effective expansion angle of 6.8 $^\circ$. At steady flow conditions the stagnation enthalpy is calculated to be 5.7 MJ/kg, the Reynolds number based on wedge length at the step is 2.0×10^5 , with the viscosity calculated using the Sutherland viscosity law.

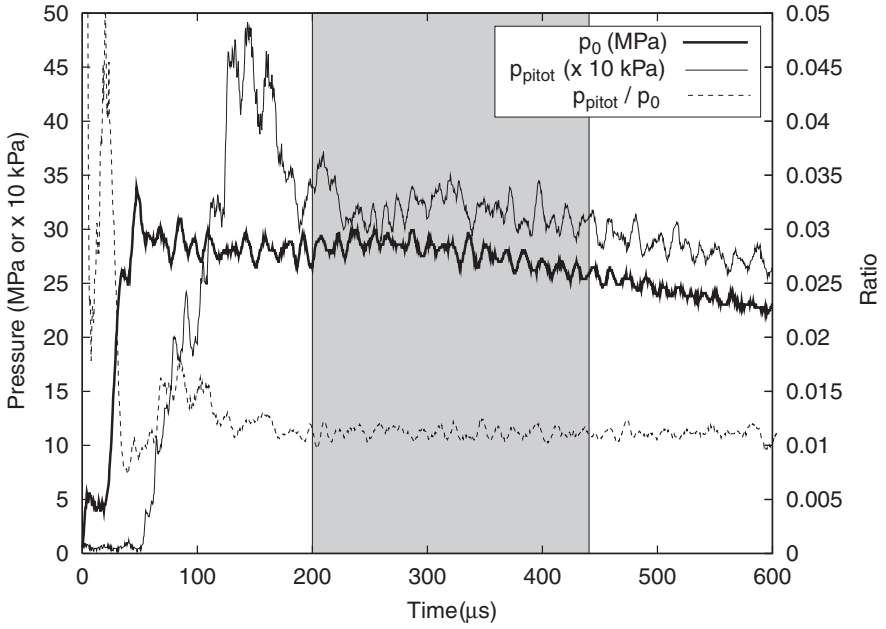

Figure 1: Typical nozzle reservoir and pitot pressure traces, with their ratio. The shaded region shows the nominal test duration.

The facility uses a conical nozzle, which causes the pressure to drop as a function of axial distance. Between the tip of the model and the end of the first horizontal plate in Fig. 2, the static pressure and static temperature drop by 50 % and 18 % respectively. The favourable axial pressure gradient caused by this nozzle expansion makes the flow less likely to undergo transition in the free shear layer immediately downstream of the step. Although this axial pressure gradient is significant, it does not change the general features of the separated flowfield when compared with a uniform freestream.

Because the available volume of the test gas in the shock tube is limited, the facility has a steady test time of around 200–250 μs, starting 150–200 μs after the shock wave reflects at the end of the shock tube. Thereafter, the reservoir pressure decreases at a rate of 2 MPa per 100 μs. The test time for the facility was limited by the establishment of the steady nozzle flow at the beginning of the test and by a drop in nozzle reservoir pressure to 80 % of the original value at the end of the test. Nozzle reservoir conditions for the nozzle exit flow were computed by accounting for the 75 μs transit time of the flow through the nozzle. Figure 1 shows a Pitot pressure and nozzle reservoir pressure trace for these conditions, to provide an indication of the test time. It should be noted that when the nozzle transit time is accounted for, the ratio of the pitot pressure to the nozzle reservoir pressure remains constant at a value of 0.011 throughout the nominal steady flow time.

The Reynolds number at these flow conditions was low enough for the flow along the wedge to be considered laminar according to the criterion of Lees [4], although several previous studies on hypersonic laminar separated flows [5–7] have indicated that laminar separated flows readily transition in the free shear layer. The visualisations presented later in the paper showed no evidence of large-scale turbulent structures in the free shear layer.

Table 1: Nozzle reservoir conditions and freestream conditions calculated at the nozzle exit.

Flow property	Nozzle reservoir value
Pressure, p_0	26.2 MPa
Temperature, T_0	4600 K
Flow property	**Nozzle exit value**
Pressure, p_∞	5.2 kPa
Temperature, T_∞	470 K
Density, ρ_∞	0.037 kgm^{-3}
Frozen Mach number, M_∞	7.5
Velocity, u_∞	3175 ms^{-1}

The experiments presented in this paper were performed on a 30 $^\circ$ half-angle wedge model. Using a wedge upstream of the step reduces the Mach number from 7.5 to 3.0 immediately upstream of the separation, assuming an equilibrium ratio of specific heats of $\gamma = 1.3$. Most previous hypersonic step flow experiments have been performed using a flat plate rather than a wedge upstream of the separation. The wedge model is shown in Fig. 2 (a), and had a 0.1 mm radius leading edge. The radius of the shoulder immediately upstream of the step was also 0.1 mm. The wedge was placed so that its leading edge would coincide with the nozzle exit during the test, on the centreline of the nozzle flow. The model contained 13 co-axial chromel/alumel thermocouples, one 5 mm upstream of the step, and the remaining 12 on the plate downstream of the step. The thermocouples were mounted in the model using epoxy resin and then sanded to ensure flush-mounting and to make the connection between the two thermocouple materials, which were separated by a thin oxide layer. The base plate behind the wedge was designed to be rotated 180 $^\circ$, allowing measurements for each thermocouple to be obtained at two streamwise positions. The positions of the transducers were staggered to allow this system to produce 24 measurement points on the surface downstream of the step. The closest thermocouple to the step was located 5 mm downstream of the step and 11.5 mm from the side wall of the model. The transducers were placed in three parallel rows of four transducers. The three rows were separated by 9 mm, and the

transducers in each of the three rows were staggered by 3 mm in the downstream direction, with 9 mm between transducers in the cross-stream direction.

The model was also designed to have variable step height. This allowed heat flux to be measured for both the separated flow past a 6 mm step and for attached flow without a step. Direct non-dimensional comparisons can therefore be made between heat flux in the separated flow and in the equivalent attached flow. This method was previously used by Chapman et al. [5] in their investigation of the heating downstream of a step in supersonic flow.

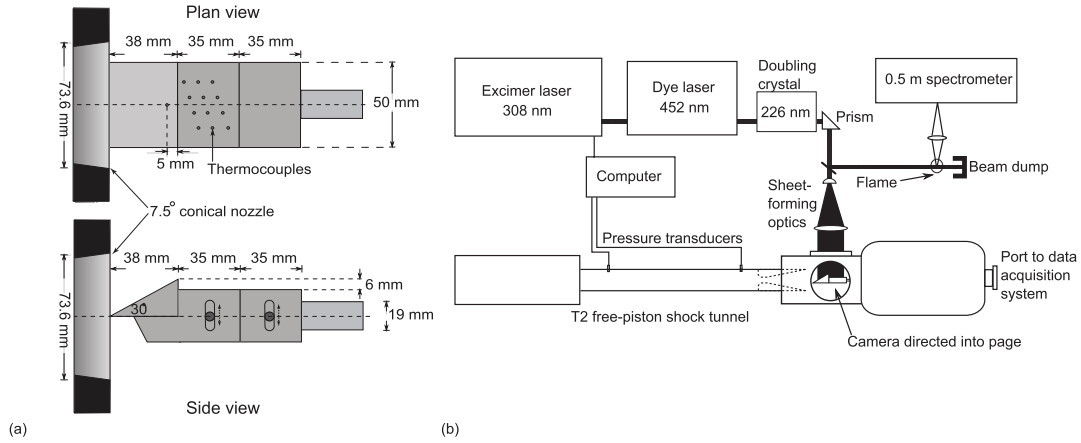

Figure 2: Schematics of (a) plan and side views of the wedge model, showing the relative positions of the model, the nozzle exit and the thermocouples; and (b) the shock tunnel and laser system.

2.2. Fluorescence Imaging System

Planar laser-induced fluorescence is a spectroscopic technique that uses a thin sheet of laser light to excite absorption transitions in a chemical species present in the flow. Part of the absorbed light is re-emitted as fluorescence and this fluorescence can be collected using a camera mounted perpendicular to the laser sheet. Nitric oxide (NO) was chosen as the excitation species in this study because it forms naturally as part of the shock-heating of the gas in the nozzle reservoir, as mentioned above.

The laser system used in the experiments is represented schematically in Fig. 2 (b). An XeCl excimer laser was used to produce light at 308 nm, which pumped a frequency-doubled dye laser, providing 3-5 mJ of light at 226 nm.

The 226 nm radiation can be used to excite electronic transitions in the $A^2\Sigma^+ \leftarrow X^2\Pi(0,0)$ vibrational band of NO. The ${}^{S}R_{21}$ (13.5) transition was chosen for excitation in this study because it is an isolated transition and provides measurable signal variation over the range of temperatures and pressures expected in the flow over the wedge.

Part of the 226 nm laser beam was re-directed through an atmospheric pressure hydrogen-air flame using a fused silica optical flat. The fluorescence generated by the flame was measured and used to calibrate the wavelength of the laser immediately before a turmel run. The main beam was passed through a -40-mm focal length cylindrical lens and a 1000-mm focal length spherical lens, to form a collimated laser sheet of 35-mm width and 0.7-mm thickness in the test section. The laser sheet was passed through the test section in one of two orientations – along the centre line in the vertical direction running perpendicular to the model's base or horizontally across the span of the model and parallel to the model's base. The fluorescence was captured using a Princeton Instruments intensified charge-coupled device (ICCD) camera, using a 100-ns gate duration. The camera used a UV-Nikkor lens with a f # of 4.5 and a focal length of 105 mm. Prior to operating the tunnel, a number of images were obtained using the same transition in a quiescent mixture of 5% NO in N_2 , to produce an image of the average laser-sheet profile. This image was used to normalise for spatial variations in laser-sheet intensity.

2.3 . Flow Establishment Experiments

Initial tests were performed to investigate the time required to establish the separated flow behind the wedge. As the shock tunnel has a limited flow duration, it is important to ensure that the time available is sufficient to establish a steady separated flow. NO PLIF visualisations were performed over several facility runs, with a different delay between the shock reflection and obtaining the image on each run. As the flow is laminar, this is a viable method of building up a time history of the flow in the absence of a laser and imaging system capable of obtaining multiple images during the 1 millisecond of flow time over a facility run. Recent experiments [8] using the resonantly enhanced shearing interferometry method developed by Hruschka et al. [9] have successfully been used to visualise flows in shock tunnel facilities at rates in excess of 100 000 frames per second. Although this technique works well, it cannot show the recirculating flow as clearly as the PLIF images do, and because shearing interferometry is a path-integrated technique, any three-dimensionality of the flow along the line of sight will contribute to the visualisation at the camera. Other recent experiments by Jiang et al. [10] have successfully acquired images of flow in a Mach 10 blow-down facility using NO PLIF at laser pulse rates of up to 1 MHz. While that work is a convincing proof of the viability of high-repetition- rate PLIF visualisation, and an excellent visualisation option for turbulent flows, the experimental arrangement used by Jiang et al. requires a custom-built pulse burst laser and an ICCD camera that can be operated at high frame rates.

To ensure that the assumption of run-to-run repeatability used in this study was valid, we obtained images multiple times for several delay times after shock reflection, and eight times at the nominal test time. These visualisations indicated that the positions of the main flow features, including the re-attachment point, changed very little at the test time, although there was some variation between tunnel runs for images obtained during the first 250 μs after shock reflection, when the flow is establishing.

As was done in the previous study of flow establishment downstream of a 45-degree blunted cone in the work of Park et al. [8] , we have used both visualisation of the flow and heat flux measurements to determine the time for the flow to establish. Heat flux establishment times are determined by the time required for the heat flux to settle to within 5 % of the steady value, should a steady value exist.

2.4 . Fluorescence Imaging of Separated Flow Uniformity

Interpreting the flow properties using the PLIF signal alone can be difficult, because signal intensity depends upon temperature, pressure, velocity component in the direction of the laser sheet and NO number density. The calculated variation of signal intensity with temperature and pressure for the ${}^{S}R_{21}$ (13.5) transition in a stationary mixture of 1 % NO in N_2 is shown in Fig. 3. Signal intensities were calculated for this plot using the method described by Danehy et al. [11]. The peak signal, neglecting attenuation due to absorption, occurs at a temperature of approximately 250 K and pressure of approximately 7 kPa, declining rapidly at lower temperatures and pressures and more gradually at higher pressures and temperatures. The velocity of the flow in the beam direction causes a Doppler shift, which reduces the overlap between the laser and the transition and therefore decreases the signal.

Despite the complex interaction between the effects of temperature, NO concentration and velocity on the PLIF signal, the signal should be constant in a region where the temperature, pressure, velocity and NO number density are constant, and any signal non-uniformity in such a region indicates non-uniformity in one of these flow parameters. The Doppler shift in the subsonic recirculating region of the flow should be small, and the freestream PLIF intensity is within 10 % across the nozzle flow on a single tunnel run [12] , although the average PLIF signal intensity can vary by up to 20 % between tunnel runs.

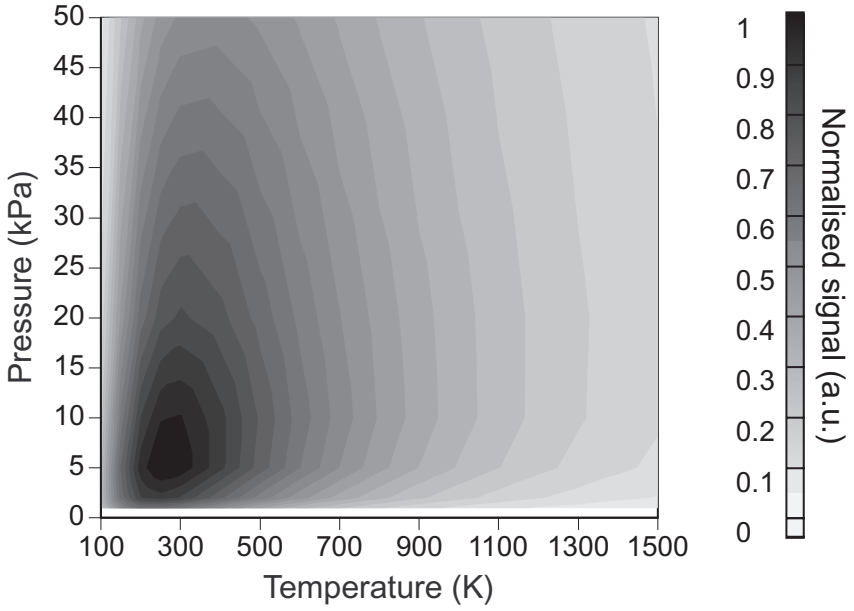

Figure 3: Variation of fluorescence intensity with pressure and temperature for the ${}^{S}R_{21}$ (13.5) transition. Signal is normalised to unity for maximum signal.

3. HEAT FLUX MEASUREMENTS

The co-axial thermocouples used in this experiment have been used in previous shock-tunnel studies of separated flow [13,14], so they are well-characterised and are resilient enough to withstand the conditions in the shock tunnel. The response time is of the order of 10 μs or less, which is sufficient to make many measurements during the steady flow time.

The signal from each of the thermocouples was passed through a pair of shielded cables to the exit of the tunnel's dump tank. The very small voltages induced by the Seebeck effect in the thermocouple, 40 µV per Kelvin for these thermocouples, makes the heat flux signal challenging to measure for the low heat flux levels in the separated flow region. Outside the tunnel differential amplifiers, each with a gain of 1500, amplified the signals sufficiently for them to be displayed and recorded using a bank of two Tektronix TDS 420 and two TDS 360 oscilloscopes. The extremely small signal amplitude and the 2 m of cable between the transducer and the amplifier generated additional noise when amplified. The cable was particularly susceptible to radio-frequency interference. For those transducers located in the separated region near the step, where the heat transfer was very low, the signal-to-noise ratio could be as low as 2 on a single run, compared to 10 or better on the wedge face and near re-attachment. This difficulty was minimised by taking an average of 12 measurements for each of the transducers, in each of the two orientations of the plate downstream of the step.

Heat flux was obtained from the temperature measurements by numerically differentiating the measured surface temperature history, assuming heat transfer to a semi-infinite substrate using the relation [15]

$$\dot{q}_n = \frac{2}{\alpha}\sqrt{\frac{\rho c k}{\pi}}\left[\sum_{i=1}^{n}\frac{V\left(t_i\right)-V\left(t_{i-1}\right)}{\left(t_n-t_i\right)^{1/2}+\left(t_n-t_{i-1}\right)^{1/2}}\right]$$

Here $V(t) = \alpha T(t)$ is the voltage output at time t, $T(t)$ is the surface temperature, α is the temperature response constant for a chromel-alumel thermocouple multiplied by the gain of the amplifier and $\sqrt{\rho c k}$ is the thermal product of the thermocouple. The thermal product was determined by previous measurements [14] to be 9800 $Jm^{-2}\,K^{-1}\,s^{-0.5}$. Results of these experiments are presented as ratios, and are independent of the values chosen for these parameters.

The calculation of heat flux resulting from Eq. 1 generates a very noisy distribution unless the

temperature data is very smooth. For this reason, the averaged temperature histories for each transducer were smoothed using a 21-point running average before the data was processed. This reduces the time resolution of the data to around 20 μs, but the temporal resolution of this data is still sufficiently high to make at least 10 measurements during the steady flow time of the facility.

4. RESULTS AND DISCUSSION

4.1. Temporal Evolution

Figure 4 shows a sequence of representative images of the wedge flow taken at times between 80 and 800 μs after the shock reflection in the nozzle reservoir. These images are of the logarithm of the signal received by the intensified camera, to emphasise the differences at low counts, as this makes the recirculating flow and shear layer appear more clearly. At 800 μs delay, the pressure in the nozzle reservoir is about 80 % of the value at the test time of 350 μs after shock reflection. The flow is from left to right. The dark region in the top and top-left of the image marks the edge of the test-section window. The wedge can be seen in the bottom-left section of each image. The images show the freestream, part of the shock layer, the expansion fan at the step and the re-attachment shock. As the laser was tuned to maximum signal at zero velocity component in the vertical direction, the bright region immediately downstream of the step contains the low-velocity recirculating flow.

The dark flow regions in the shock layer that are visible at a delay of 800 μs may be due to the arrival of the facility's argon driver gas during the tunnel run. Alternatively, they may be due to entrainment of cold gas from the nozzle reservoir, which has been noted in a previous study [12]. It was not apparent in all of the images obtained at that time, although the thicker wake neck apparent in the 800 μs image was observed in all images obtained with that time delay.

The highest PLIF signals occur in the 470-K freestream flow and in the expansion fan, while the lowest signals occur in the expanded flow downstream of the step and adjacent to the shear layer. As predicted in Fig. 3, the signal in the shock layer should be reduced to approximately 10 % of the peak signal downstream of the forebody shock wave caused by the 30 $^\circ$ wedge. This is consistent with the signal reduction in the 350 μs-delay image in Fig. 4.

The low signal in the region below the expansion is mostly caused by Doppler shift of the transition away from the excitation frequency, as computations of laminar conical base flows at similar freestream conditions [16] indicate that the temperature and density are not lower than that in the re-circulating fluid for flows over a cone at the same conditions. The lower signal in this part of the shear layer allows the slow (and therefore not significantly Doppler-shifted) re- circulating fluid to be clearly seen in the image as a region of high signal intensity.

The shock angles and the location of the wake neck can be measured directly from the images in Fig. 4 to determine the variation in these quantities during the run time of the facility. This was done for a total of 21 images for the wedge flow, obtained at times between 80 and 800 μs after shock reflection. It was found that for both model geometries, the positions of the main flow features, including the re-attachment point, changed very little for several images obtained at delays between 300 and 400 μs after shock reflection, although there was some variation between tunnel runs for images obtained during the first 250 μs after shock reflection, when the flow is establishing.

The sequence of images in Fig. 4 indicate that the re-attachment point moves downstream as the flow establishes and as it dies away, with a period of stability between these times. The re-circulation region fills during establishment and, in the latter stages of the flow, moves downstream due to the decrease in freestream pressure causing an increase in the boundary layer thickness at the step. The wake neck also thickens considerably in the latter stages of the flow, due to the thickening of the upstream boundary layer.

Figure 5 summarises the variation in both the forebody shock angle and the location of the wake neck over this time interval. Plots have been provided for the wedge with a 6-mm step and the equivalent cone with step, for comparison with the wedge results. As the cone flow is axially symmetric, there is no problem with flow spillage from the subsonic flow downstream of the step as there is for the wedge flow. Figure 5 (a) is a plot of the forebody shock angle for the wedge and cone models as a function of time. For the conical model, the flow produces a shock with an angle close to that predicted by theory after about 100 μs and the shock remains at this angle throughout the test. The shock angle for the wedge flow, on the other hand, appears to oscillate during the flow time. This may have been because the 50-mm width of the wedge is closer to the edge of the nozzle core flow diameter, which potentially causes the wedge shock to be affected by the nozzle boundary layer. In both cases, at

the test time, the angle of the forebody shock is within measurement uncertainty of the shock angle predicted by inviscid compressible flow theory.

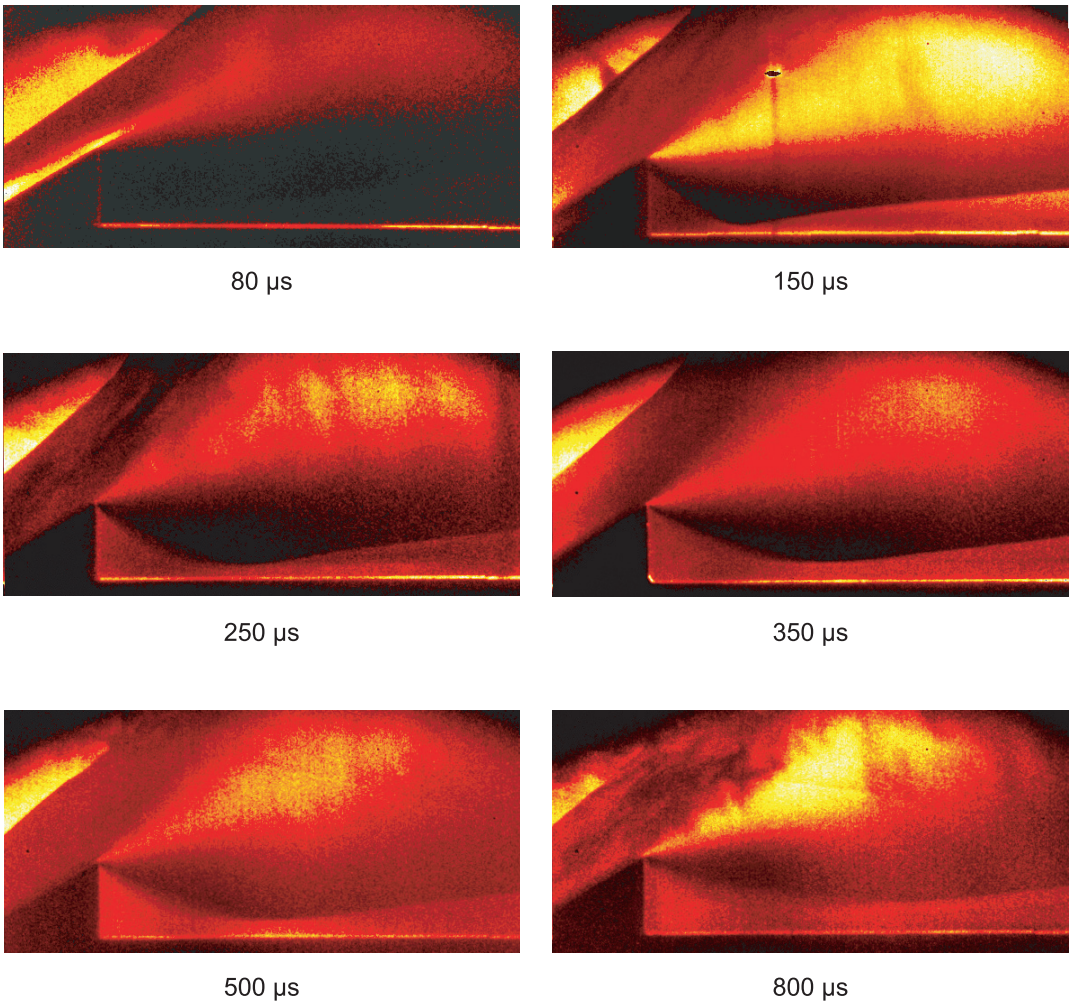

Figure 4: NO PLIF images of the wedge near-wake flow at various times after shock reflection in the nozzle reservoir.

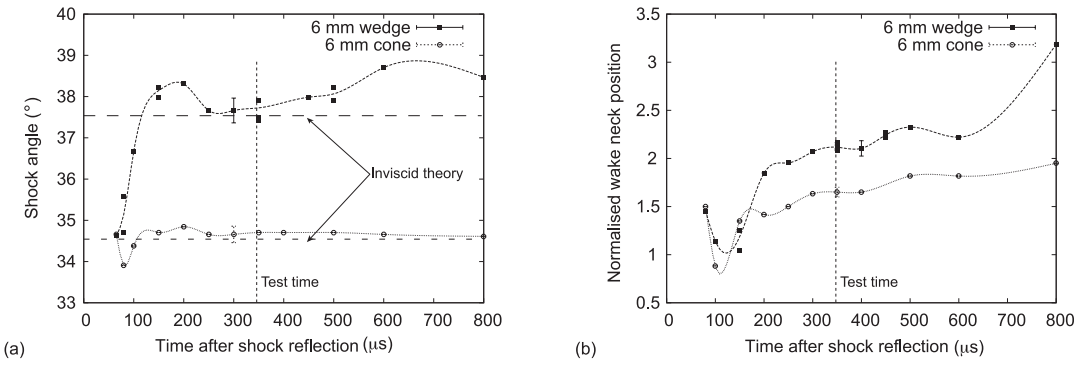

Figure 5: Variation with time of (a) the shock angle and (b) the wake neck location, normalised to the step height.

Figure 5 (b) is a plot of the re-attachment position downstream of the step, normalised to the step height, as a function of time after shock reflection. The trends for each model geometry are equivalent, with the wedge's separated region being further from the base than the position for the equivalent cone. The wake neck is also 30% thicker for the wedge than for the equivalent cone. For both geometries in Fig. 5 (b), there is a time window between 300 and 400 μs after shock reflection for which the distance of the re-attachment point from the base does not appear to vary. This indicates that the separated region has reached a steady state during that time. Heat flux measurements for a 12.5-mm conical step at the same freestream conditions indicate that the re-attachment point did not reach a steady value during the test time but kept increasing. The flow establishment criterion determined by Holden [17] indicates an establishment time of more than 400 μs for the 12.5-mm step, but only around 200 μs for a 6-mm step, based upon the flow external to the shear layer moving 50 base heights downstream during establishment.

4.2. Flow Uniformity

The results of the spatial flow uniformity experiment are summarised in Fig. 6. Fig. 6(a) and (b) are PLIF images of the flow, showing the important flow features between the step and the boundary layer re-attachment point. Fig. 6(a) is a PLIF image of the flow along the centre-line of the model, obtained during the nominal test time, 350 μs after shock reflection.

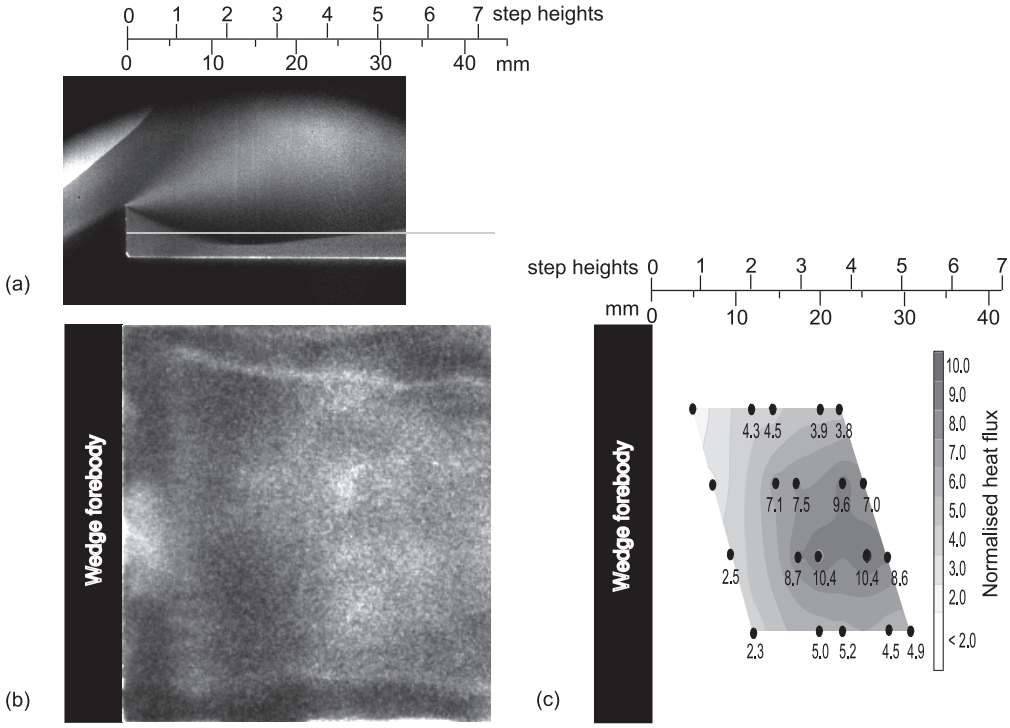

Figure 6: Fluorescence images and heat flux distribution. Flow in each case is from left to right, and the laser sheet propagates from the top to the bottom of the images. The distance scales are the same for each of the images. (a) Side view of the flow at the centre of the model. (b) View from above, with horizontal laser sheet located 3 mm above the surface. (c) Surface plot of the heat flux distribution at the base of the wedge.

The horizontal line running through Fig. 6(a) indicates the approximate position of the laser sheet used to generate the span-wise PLIF image of Fig. 6(b). This image shows the flow features in a horizontal slice 3 mm above the base plate. The flow shown in Fig. 6(b) is quite complex, but the main flow features are apparent. At the top and bottom of the image, bright curved lines indicate the expansion of flow around the sides of the plate. The shear layer is seen as a bright vertical line near the left of the image, approximately 1.2 base heights downstream of the step. The re-circulating flow occurs

to the left of this line. The re-attached flow corresponds to the bright region between 3.8 and 4.2 base heights, and the intersection of the image plane with the re-compression shock is quite diffuse. Fig. 6(b) shows the re-circulating vortex region to be highly non-uniform. The shear layer is apparent as a brighter region immediately downstream of the vortex. The re-attachment shock shown in Fig. 6(b) appears to be upstream of the position in Fig. 6(a), occurring between 4 and 4.5 base heights downstream of the step. The difference is most likely due to an inclination in the horizontal laser sheet. The run-to-run variation in the position of the re-attachment in Fig. 6(a) was less than 10% over 8 images. The re-attachment shock also appears more diffuse in the horizontal plane than in the vertical plane, perhaps due to imperfect focussing on the laser sheet. Two streamwise vortices arising from the edges and upper comers of the step are visible in Fig. 6(b).

The non-uniformity of the flow in the re-circulating region of Fig. 6(b) is apparent, with high signal in the centre of the region and much lower intensity at the edges. A clearer indication of this non-uniformity is shown in Fig. 7. This figure contains two plots of the spanwise distribution of fluorescence intensity shown in Fig. 6(b), averaged over 15 pixels in the horizontal direction. The heavy line is the signal distribution across the re-attachment zone 5 base heights downstream of the step, while the light line represents the fluorescence intensity across the re-circulating region 0.3 base heights downstream of the step. The intensity in the re-attachment zone is constant to within 20 % over the central two-thirds of the span, indicating that the flow downstream of re-attachment is reasonably uniform in the central part of the wedge flow. In the re-circulating zone a region of low signal, caused by a combination of low density and possibly Doppler shift, occurs at the top and bottom of the image. This indicates the escape of flow from the subsonic re- circulating flow, towards the sides of the model. A region of relatively high PLIF intensity occurs in the middle of the plot, corresponding to the re-circulating region in Fig. 6(a). The signal in this region does not reach a plateau, however, so the assumption of two-dimensionality appears to be invalid for the re-circulating flow. The intensity distribution is also slightly asymmetric, with the peak being closer to the bottom of the image than to the top. This is possibly due to detuning of the laser from the zero-velocity line centre for this image. The fact that other studies have been undertaken with smaller model aspect ratios [18] emphasises the importance of careful flow uniformity measurements. As this region is the one where the lowest signal-to-noise ratios occur for heat flux measurements, the PLIF imaging forms a very useful complement to heat flux measurements.

Figure 6(c) shows the distribution of the average heat flux across and along the plate downstream of the wedge. The filled circles indicate the position of transducers used in the measurements. The numbers indicate the averaged heat flux measured by each transducer during the steady flow time as a percentage of the flux measured by the forebody transducer. The contour map is a two-dimensional linear interpolation between the measured values, providing a general indication of the heat flux distribution between the transducers. The flux varies between 2 % and 10 % of the forebody transducer's heat transfer. Two of the transducer measurements are not shown because the signal-to-noise ratio was less than 2. These transducers were located close to the step, where the heat flux was too low to measure accurately. The standard deviation of the average heat flux varied from 5 % to 20 % of the signal during the test time, depending on the position of the transducer. Measurements for transducers with high signals and small measurement uncertainties showed a run-to-run heat flux fluctuation of approximately 10 % over 12 facility runs. The maximum heat flux occurs between 3.3 and 4.4 step heights downstream of the step, depending on spanwise location. This is downstream of the wake neck, which occurs approximately 2.2 step heights downstream of the step, based on the PLIF images. The heat flux reduces downstream of this point, because the flow has turned parallel to the plate and because the freestream expands with distance downstream of the conical nozzle.

As one might expect, the heat flux decreases at the outer edges of the plate due to flow spillage, but the heat flux seems to be reasonably uniform in the re-attachment region, a result that is consistent with the PLIF visualisation in Fig. 6(c). The heat flux measurements are not sensitive enough to make any conclusive statements about the spanwise heat flux distribution in the re-circulating region, except to say that the heat flux is around 20–25 % of the peak heat flux downstream of reattachment at the two points where the heat flux was large enough to be measured.

4.3. Peak Heat Flux Measurements

It is informative to compare heat flux measurements in separated flow with those experienced by an equivalent attached flow [19], as this is a useful indication of the effect of separation on surface heat

transfer. Experiments performed by Rom and Seginer [20] have shown that the ratio of the maximum heat flux downstream of a step to that for an equivalent attached flow correlates with the quantity $L/\left(hRe_L^{1/2}\right)$. For a laminar flow, this quantity is a dimensionless representation of the ratio of the thickness of the attached boundary layer immediately upstream of the step to the step height. According to their study, flows where this parameter is greater than 0.067 have thick incoming boundary layers and cause the heat transfer rise to approach a gradual maximum value, while flows where $L/hRe_L^{1/2} < 0.067$ have a relatively thin oncoming boundary layer and are characterised by a sharp peak in heat flux near the re-attachment point, with the ratio $\dot{q}/\dot{q}_{fp}$ reaching 7 for the smallest measured value of $L/hRe_L^{1/2} = 0.02$.

Heat flux with no step was measured at the same position as the heat flux measured with a 6-mm step, providing a ratio that can be directly compared to previous experiments [13,18,20,21], and to the correlation of Rom and Seginer. In these experiments, the no-step heat flux was obtained by moving the horizontal plate upwards until it was level with the corner of the wedge. The value of $L/\left(hRe_L^{1/2}\right)$ for this experiment was 0.016, calculated using the post-shock flow parameters based upon the calculated freestream conditions and the oblique shock relations. The measured maximum heat flux ratio for this study was 1.7 times that for the equivalent attached boundary layer. A summary of the relevant parameters in all three experiments is provided in Table 2. The normalised peak heat flux measured in this experiment agrees well with the value of 2.0 measured by Gai et al. It should also be noted that experiments performed by Wada and Inoue 18 show peak heat flux values around twice that of the equivalent attached boundary layer value, in good agreement with the peak heat fluxes measured in the present study. Both these results, and those of the present study, disagree with the results and correlation of Rom and Seginer. The gradual nature of the distribution of heat flux with downstream distance is also in agreement with the other studies listed in Tab. 2, and in contrast with the distinct peak in the distribution measured by Rom and Seginer for the same value of $L/\left(hRe_L^{1/2}\right)$.

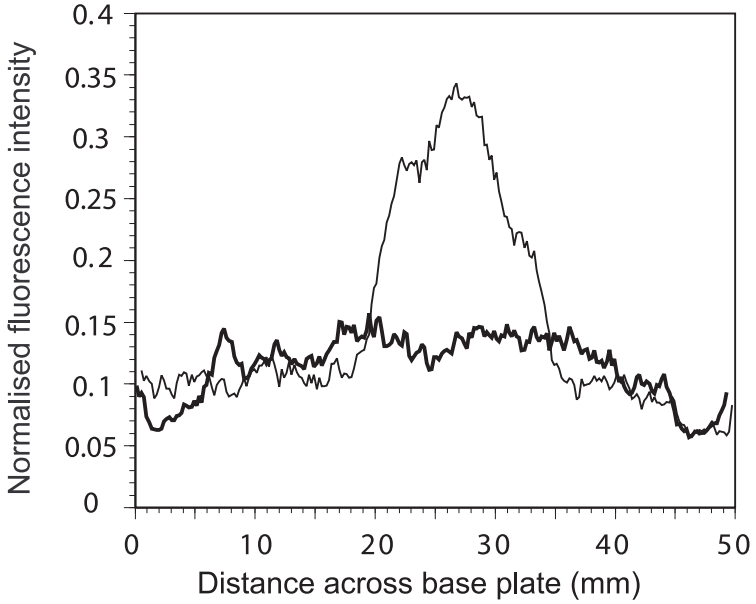

Figure 7: Cross-section of the fluorescence intensity from Fig. 6 in the re-circulating region, 0.3 base heights down-stream of the step (thin line) and in the re-attachment zone (thick line), 5 base heights downstream of the step.

None of the flow conditions presented in Tab. 2 have high-enough stagnation enthalpy to produce significant real- gas effects on the heat transfer. Although the present results and those of Gai et al. have a vibrationally excited freestream, any influence of this would be to increase the heat flux compared to a flow with the same internal energy in vibrational equilibrium.

The aspect ratio for the present experiment, defined as the ratio of span to length along the wedge

surface upstream of the step, is smaller than that of the other studies. This was done deliberately to emphasise the effect of the aspect ratio on the PLIF uniformity images. Additionally, neither the present experiments nor those of Gai et al. used sideplates to minimise spillage. The non-uniformity in the re-circulating region shown by Fig. 6 (b) means that caution must be exercised when comparing with Rom and Seginer's correlations. However, the effect of lower density in the re-circulating region would be to increase the deflection angle of the shear layer and bring the re-attachment point closer to the step. This should have the effect of increasing the temperature gradient in the reattaching shear layer, thereby increasing peak heat release. This trend is opposite to the difference between the maximum measured flux in the present experiment and that of Rom and Seginer.

The most obvious difference between the conditions in Rom and Seginer's experiments and those of the other studies is the Mach number, which is supersonic in the former case and hypersonic for the latter cases. For cold-wall cases, the hypersonic flows will generate a distinct peak temperature in the boundary layer that is much higher than that in either the external flow or at the wall. This effect is much smaller in the case of the supersonic flow of Rom and Seginer. The heating of the surface due to the impingement of the shear layer at the wall is likely to be higher as a proportion of the attached flat plate heating for the supersonic flow, as the latter is much lower in the supersonic flow.

Table 2: Comparison of flow conditions and peak heat flux measurements between the present experiment and two previous studies [13,20].

	Rom and Seginer[20]	Wada and Inoue[18]	Gai et al.[13]	Hayne[21]	Present Study
H_0 (MJ/kg)	unknown	1.5	2.6	5.6	5.7
M_∞	1.5 – 2.5	10.4	10.1	6.1	7.5
Model aspect ratio	5.4	1 – 5	4.0	4.13	1.14
T_w/T_0	0.02 – 0.3	0.24–0.28	0.13	0.065	0.064
h (mm)	1.55	3–5	6.0	2.2	6.0
Re_L	200 000	65 000–450 000	233 000	141 600	205 000
$L/\left(hRe_L^{1/2}\right)$	0.02	0.013–0.045	0.017	0.029	0.016
$\left(\frac{\dot{q}}{\dot{q}_{fp}}\right)_{max}$	4.85	0.9–1.9	2.0	1.0	1.7 ± 0.2

5. CONCLUDING REMARKS

Both planar laser-induced fluorescence and thermocouple sensors have been used to examine the establishment and the two-dimensionality of the flow in the near wake and re-attachment zone for flow past a wedge with a rearward-facing step. The PLIF images show that the recirculating region in the centre of the wedge and the flow downstream of that point reaches a steady state during the nominal 350 μs test time of the facility. Both PLIF and heat flux measurements give similar indications of the two-dimensionality downstream of the re-attachment, but PLIF gives a much more sensitive indication of the degree of uniformity in the re-circulating region, where the thermocouple signals were too small to be properly resolved. The PLIF images show that the flow in the re-circulating region is non-uniform, and this may cause disagreements between measured data and two-dimensional correlations or flow simulations.

The maximum heat flux results were normalised to the equivalent heat flux for an attached flow, and compared with the results of Rom and Seginer, Wada and Inoue, Gai et al. and Hayne. Despite the very low aspect ratio in the current experiment, which makes the recirculating flow highly non-uniform, the peak heat flux ratio and the form of the heat flux distribution agrees well with those of Gai et al., Wada and Inoue and Hayne at similar values of $L/\left(hRe_L^{1/2}\right)$.

This indicates that three-dimensionality of the separated flow does not have a strong effect on the peak reattaching heat flux. The heat flux measurements disagree with the equivalent measurements and correlation of Rom and Seginer. The reason for this disagreement is postulated to be due to the lower total enthalpy and freestream Mach number for Rom and Seginer's study. A higher Mach number

generates a strong peak temperature in the upstream attached boundary layer, and hence also in the free shear layer. This effect dominates that of the reattaching flow on the peak heating at high freestream Mach numbers.

REFERENCES

[1] Stalker, R. J. The Free-Piston Shock Tunnel. *AIAA Journal*, 5(12), 34–38, 1967.

[2] McIntosh, M. Computer Program for the Numerical Calculation of Frozen Equilibrium Conditions in Shock Tunnels. Tech. Report, Department of Physics, Faculties, Australian National University, 1968.

[3] Vardavas, I. Modelling Reactive Gas Flows within Shock Tunnels. Australian Journal of Physics, 37, 157–77, 1984.

[4] Lees, L. Hypersonic Wakes and Trails. *AIAA Journal,* 2(3), 417–528, 1964.

[5] Chapman, D. R., Kuehn, M. and Larson, K. Investigation of Separated Flows in Supersonic and Subsonic Streams with Emphasis on the Effect of Transition. Technical report, NACA TR 1356, 1958.

[6] Hollis, B. R. and Perkins, J. N. Transition Effects on Heating in the Wake of a Blunt Body. Journal of Spacecraft and Rockets, 35(5), 668–674, 1999.

[7] Hruschka, R., O'Byrne, S. and Kleine, H. H. Comparison of Velocity and Temperature Measurements with Simulations in a Hypersonic Wake Flow. *Experiments in Fluids,* 51, 407–421, 2011.

[8] Park, G., Hruschka, R., Gai, S. L. and Neely, A. J. Flow Establishment behind Blunt Bodies at Hypersonic Speeds in a Shock Tunnel. In *Proc. of SPIE Vol. 7126*. 2009. doi:10.1117/12.822751.

[9] Hruschka, R., O'Byrne, S. and Kleine, H. Diode-Laser-Based Near-Resonantly Enhanced Flow Visualization in Shock Tunnels. *Applied Optics,* 47(24), 4352–4360, 2008. doi:10.1364/AO.47.004352.

[10] Jiang, N., Webster, M., Lempert, W. R., Miller, J. D., Meyer, T. R., Ivey, C. B. et al. MHz-Rate Nitric Oxide Planar Laser-Induced Fluorescence Imaging in a Mach 10 Hypersonic Wind Tunnel. Applied Optics, 50(4), A20–A28, 2011. doi:10.1364/AO.50.000A20.

[11] Danehy, P., Palma, P., Boyce, R. and Houwing, A. Numerical simulation of laser-induced fluorescence imaging in shock-layer flows. *AIAA Journal*, 37(6), 715–23, 1999.

[12] O'Byrne, S. B., Danehy, P. M. and Houwing, A. F. P. Investigation of Hypersonic Nozzle Flow Uniformity using NO Fluorescence. *Shock Waves,* 15(2), 81–87, 2006.

[13] Gai, S., Reynolds, N., Ross, C. and Baird, J. Measurements of Heat Transfer in Separated High-Enthalpy Dissoci- ated Laminar Hypersonic Flow behind a Step. *J. Fluid Mech.,* 199, 541–61, 1989.

[14] Mallinson, S., Gai, S. and Mudford, N. The Interaction of a Shock Wave with a Laminar Boundary Layer at a Compression Corner in High-Enthalpy Flows Including Real-Gas Effects. Journal of Fluid Mechanics, 342(10), 1–35, 1997.

[15] Schultz, D. and Jones, T. Heat-Transfer Measurements in Short-Duration Hypersonic Facilities. AGARDograph AGARD-AG-165, Advisory Group for Aerospace Research and Development, 1973.

[16] O'Byrne, S. Hypersonic Laminar Boundary Layers and Near-Wake Flows. Ph.D. thesis, Australian National University, 2002.

[17] Holden, M. S. Establishment Time of Laminar Separated Flows. *AIAA Journal,* 9(11), 2296–2298, 1971.

[18] Wada, I. and Inoue, Y. Heat Transfer Behind the Backward Facing Step in the Hypersonic Flow. In International Symposium on Space Technology and Science, 425–32. Tokyo, 1973.

[19] Larson, H. K. Heat Transfer in Separated Flow. Journal of the Aerospace Sciences, 26(11), 731–38, 1964.

[20] Rom, J. and Seginer, A. Laminar Heat Transfer to a Two-Dimensional Backward Facing Step from the High- Enthalpy Supersonic Flow in the Shock Tube. *AIAA Journal,* 2(2), 251–55, 1964.

[21] Hayne, M. J. *Hypervelocity Flow over Rearward-Facing Steps*. Ph.D. thesis, University of Queensland, 2004.